PEAK CURRENT OPTIMIZATION FOR LCLS BUNCH COMPRESSOR 2

A. Kabel, P. Emma
SLAC, Stanford, CA 94309, USA*

INTRODUCTION

In this study, we calculate the effects of Coherent Synchrotron Radiation (CSR) in the LCLS bunch compression section BC2[3] on the resulting FEL performance, considering a realistic, strongly non-gaussian longitudinal charge distribution. The longitudinal chirping required for the bunch compression process leads to a non-linear, non-monotonous $\delta(z)$ functional dependence (Fig. 1 shows the current distribution and the energy offset along the bunch). We model this functional dependence by matching it to a cubic polynomial $\delta \approx c_0 + c_1 z + c_2 z^2 + c_3 z^3$. During compression, the charge distribution in the $z-\delta$ plane will 'fold over', as shown in fig. 2. This leads to a cusp at each end of the current distribution $I(z)$, as shown in figure 3. High $|I'(z)|$ values will lead to high longitudinal CSR fields, with possible detrimental effects on the transverse projected and slice emittance as well as energy spread, possibly affecting FEL performance.

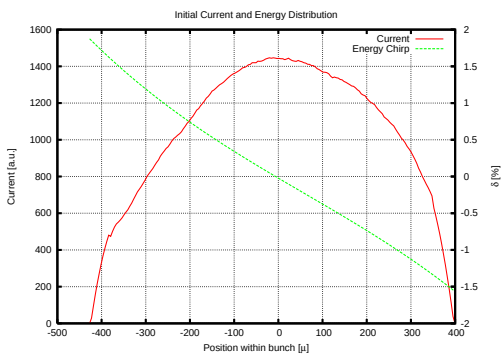

Figure 1: Initial longitudinal current and energy distribution within the bunch at 4.54GeV

SIMULATIONS

The parameters for the BC2 chicane used in our simulations are given in table 1.

For our study, we use the simulation code TraFiC^4[1]. The code has been extended for this study to allow for arbitrary, user-specified charge distributions.

In our study, we typically populate the bunch with a resolution of $3\times3\times1\times1\times768\times1$ in x,x',y,y',z,δ. y is unimportant, as the problem is essentially two-dimensional. The δ distribution is dominated by the δ,z correlation; its uncorrelated component is modeled by giving the macroparticles a length of $R_{56}\sqrt{\langle\delta^2\rangle_{uncorr}}$. This, and the need for a faithful modeling of the compression process, leads to the high

* Work supported by U.S. Department of Energy, contract DE-AC03-76SF00515.

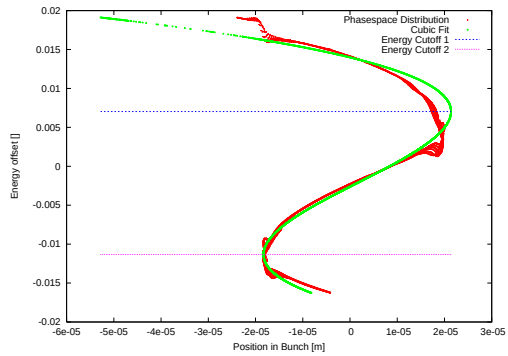

Figure 2: Particle distribution in the z-δ plane after BC2 at 4.54 GeV; weight of particles not shown. Also shown are the final cubic fit to the $\delta(z)$ distribution and the resulting energy cutoff points.

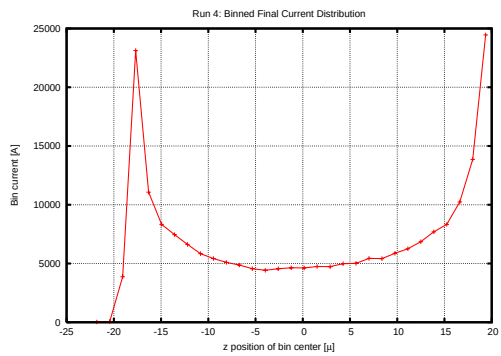

Figure 3: Formation of current cusps: Final longitudinal current distribution within the bunch. The final bunchlength in this particular case is $\sigma_z = 13.7\mu$

.

number of particles required in the longitudinal direction. Also, we prepared a sampling bunch of vanishing longitudinal dimension in the longitudinal center of the bunch. Its x,x',y,y' distribution is chosen according to the initial Twiss parameters, it is populated with (typically) 1000 particles of equal weight. We convinced ourselves that the induced emittance growth in that central slice is benign in each case.

The beamline was divided into $5\ldots8$ slices per element. In all, we have to deal with a total number of $4\cdot10^9$ three-dimensional integrations over the retarded charge distribution of a macroparticle. To our knowledge, this is the highest resolution run ever done with TraFiC^4. Clearly, the use of parallel computing is required. We used a cluster of 256 IBM CPUs at the Department of Energy's NERSC facility.

We ran a total of six cases. The final bunchlength is determined by the inital value of the linear energy chirp; how-

Table 1: LCLS BC2 parameters. The linear chirp c_1 will be varied. * refers to initial value(s)

Parameter	Symbol	Value	Unit
Bunch Charge	Ne	1.0	nC
e^- Energy	E_0	4.54	GeV
RMS Energy Spread			
correlated*	σ_E/E_0	0.72	%
uncorrelated*	σ_{Eu}/E_0	0.003	%
RMS bunch length			
initial*	σ_{z_0}	195	μm
final	σ_{z_f}	21	μm
Norm. x-emittance*	$\gamma\varepsilon_x$	1.0	μm
Norm. y-emittance*	$\gamma\varepsilon_y$	1.0	μm
Momentum Cmpctn.	R_{56}	-24.7	mm
Bend Angle per Dipole	$\lvert\theta\rvert$	34.55	mrad
Bend Magnet Length	L_B	0.500	m
Drift Bend 1(2)—2(4)	ΔL	10.0	m
Drift Bend 2—3	ΔL_c	1.00	m
Peak Dispersion	$\lvert\eta_{pk}\rvert$	363	mm
Beta Function*	β_x, β_y	115, 20	m
Alpha Function*	α_x, α_y	5.3, 0.17	
Energy Chirp*	c_1	33.71	m^{-1}
2nd-order Chirp*	c_2	6092	m^{-2}
3rd-order Chirp*	c_3	$3.477\cdot10^7$	m^{-3}

Table 2: Nominal LCLS FEL parameters.

Parameter	Symbol	Value	unit
e^- Energy in Undulator	E_u	14.1	GeV
Undulator Period	λ_u	3	cm
Undulator Parameter (peak)	K	3.64	
FEL Parameter	ρ	4.5	10^{-4}
Rad. Wavelength	λ_r	1.5	Å
Mean Beta Function	$\langle\beta_u\rangle$	26	m
RMS Energy Spread	σ_E/E_u	0.01	%
Peak Current	I_{pk}	3.2	kA
Norm. Transv. Emitt.	$\gamma\varepsilon_{x,y}$	1.0, 1.0	μm

ever, it has to be determined numerically as CSR-induced energy spread will influence the results. In our cases, the final rms bunch lengths were 18.5, 16.0, 13.7, 11.5, 10.6, and 9.6μm; the design value is 21.0μ.

POSTPROCESSING

TraFiC[4] outputs the phasespace coordinates and weights of the macroparticles and sampling particles used in the run. We are interested in the longitudinal phasespace distibution in the last timestep.

In the FEL process, only particles within a length of $\approx 0.5\mu$ cooperate, thus, to quantify the performance of the FEL, slices of this length can be treated independently. They can be characterized with sufficient accuracy by their charge, rms length, energy width, and transverse emittance.

Naively slicing distributions such as the one in fig. 2 would lead to slices with huge energy spreads, as the distribution within a slice is concentrated around two branches with an energy distance far greater than the width of the branch. Therefore, the temporally leading and trailing branches of the z-δ distribution will be cut off and disregarded in our further considerations. In the FEL process, slices from these branches would lase independent from slices from the central branch. To find appropriate cut-off points, the distribution is approximated by a function $z(\delta) = a\delta^3 + b\delta^2 + c\delta + d$, the coefficients are fitted with a non-linear least-square methods to the datapoints, using the particle charges as relative weights. From this, we find the cutoff energies at $\delta_\pm = \frac{\pm\sqrt{b^2-3ac}-b}{3a}$. Disregarding all particles with energies without the range $[\delta_+, \delta_-]$, we divided the distribution in 16 longitudinal slices. The z-δ distribution has a strongly correlated center; in accelerator stages downstream from the bunch compressors, the linear part of this correlation will be eliminated by wakefields. A good approximation for the linear correlation coefficient is given by $1/c$. Furthermore, the relative energy deviation will be reduced due to adiabatic damping. We will thus use an 'Undulator' energy deviation $\delta_U = \frac{\gamma_{BC}}{\gamma_U}(\delta - z/c)$, with relativistic γ_{BC}, γ_Us for Bunch Compressor and Undulator. We proceed by calculating the correlation matrix $\langle(x,x',z,\delta_U)\otimes(x,x',z,\delta_U)\rangle$ in each bin. We separate the energy spread into an uncorrelated and a correlated part according to $\langle\delta_U^2\rangle_{\text{corr}} = \langle\delta_U z\rangle^2/\langle z^2\rangle$, $\langle\delta_U^2\rangle_{\text{unc}} = \langle\delta_U^2\rangle - \langle\delta_U^2\rangle_{\text{corr}}$. As the bin length $\Delta z_{\text{bin}} > \Delta z_{\text{slippage}}$, the effective energy spread of a longitudinal bin for purposes of FEL performance is given by

$$\sqrt{\langle\delta_U^2\rangle_{\text{eff}}} = \sqrt{\langle\delta_U^2\rangle_{\text{unc}}} + \frac{\Delta z_{\text{bin}}^2}{\Delta z_{\text{slippage}}^2}\langle\delta_U^2\rangle_{\text{corr}} \qquad (1)$$

All needed quantities can be extracted from the correlation matrix. They are then substituted into the expressions given in [2], using undulator parameters given by table 2, and the FEL saturation power and gain length is calculated. As the y emittance ε_y will be constant and in general be different from ε_x, we use their quadratic mean as an effective transverse emittance.

RESULTS AND CONCLUSIONS

The resulting figures for FEL saturation power and gain length, slice energy spread and offset, transverse emittance, and relative weight are displayed in figs. 4—8. They indicate clearly that slice emittance will be well preserved in the center of the bunch down to 9.6μ final bunch length. Slice saturation power continues to increase and saturation length continues to decrease to that length. Further studies should aim at establishing the break-even point in final bunch length, which may be well below the shortest bunch-length considered here.

REFERENCES

[1] A. Kabel, M. Dohlus, T. Limberg; NIM-A 455 (2000),185-9

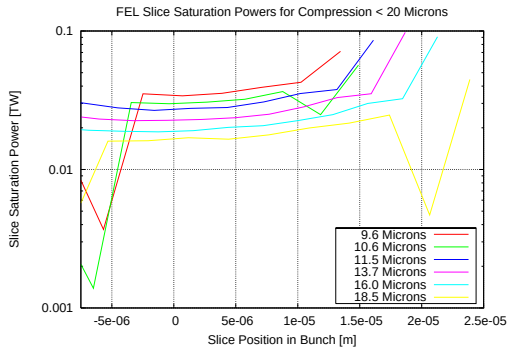

Figure 4: Resulting saturation power ($\approx 20 \ldots 40$GW in the center range) for each longitudinal slice for each final bunchlength. The actual number of slices shown is < 16, as the range has been restricted to the center of the bunch.

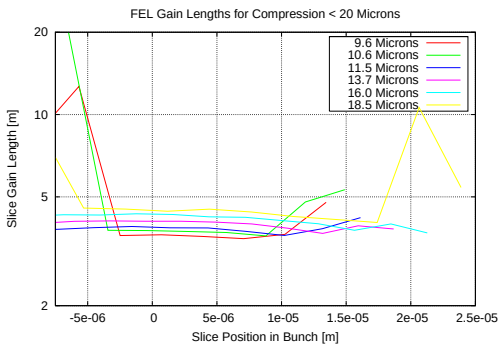

Figure 5: Resulting gain lengths ($\approx 4.5 \ldots 3.5$m in the center range) for each longitudinal slice for each final bunchlength. The actual number of slices shown is < 16, as the range has been restricted to the center of the bunch.

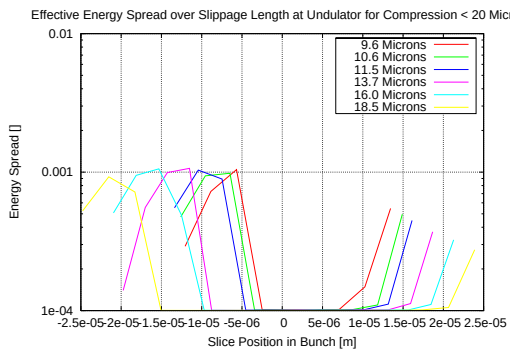

Figure 6: Resulting effective energy width at undulator over a slippage length for each longitudinal slice for each final bunchlength.

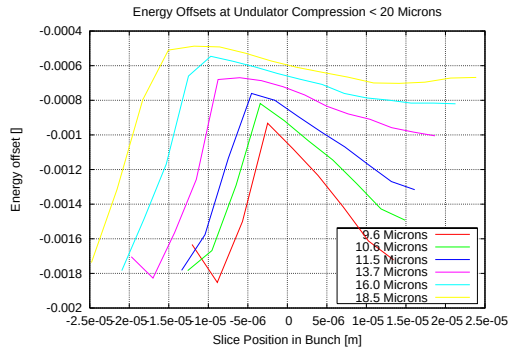

Figure 7: Resulting energy offset at undulator for each longitudinal slice for each final bunchlength.

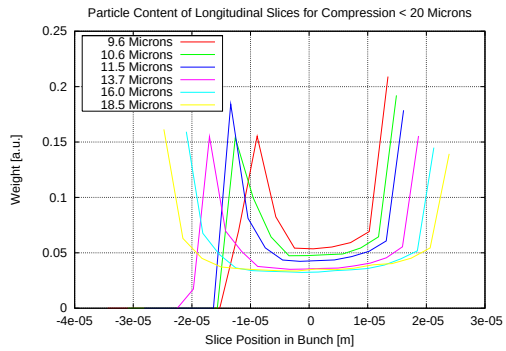

Figure 8: Particle content of slices at undulator for each longitudinal slice for each final bunchlength (normalized).

[2] M. Xie, *Design optimization for an X-ray free electron laser driven by SLAC linac*. Proc. 16th IEEE Particle Accelerator Conference (PAC 95)

[3] LCLS CDR, SLAC Report No. SLAC-R-593, 2002.

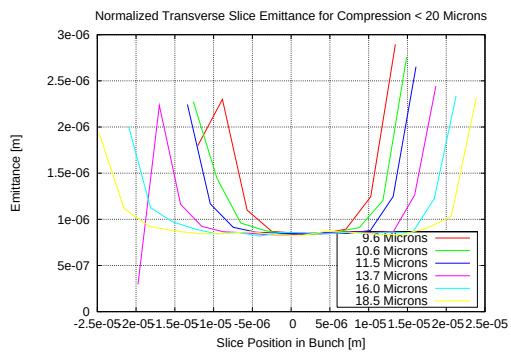

Figure 9: Normalized transverse slice emittance at undulator for each longitudinal slice for each final bunchlength. Note that the transverse emittance will be slightly underestimated due to the low number of particles in each slice.